The Canadian Mineralogist
Vol. 56, pp. 235-245 (2018)
DOI: 10.3749/canmin.1800002

AMMONIOZIPPEITE, A NEW URANYL SULFATE MINERAL FROM THE BLUE LIZARD MINE, SAN JUAN COUNTY, UTAH, AND THE BURRO MINE, SAN MIGUEL COUNTY, COLORADO, USA

ANTHONY R. KAMPF[§]

Mineral Sciences Department, Natural History Museum of Los Angeles County, 900 Exposition Boulevard, Los Angeles, California 90007, U.S.A.

JAKUB PLÁŠIL

Institute of Physics ASCR, v.v.i., Na Slovance 1999/2, 18221 Prague 8, Czech Republic

TRAVIS A. OLDS

Department of Civil and Environmental Engineering and Earth Sciences, University of Notre Dame, Notre Dame, Indiana 46556, U.S.A.

BARBARA P. NASH

Department of Geology and Geophysics, University of Utah, Salt Lake City, Utah 84112, U.S.A.

JOE MARTY

5199 E. Silver Oak Road, Salt Lake City, Utah 84108, U.S.A.

ABSTRACT

The new mineral ammoniozippeite (IMA2017-017), $(NH_4)_2[(UO_2)_2(SO_4)O_2]\cdot H_2O$, was found in both the Blue Lizard mine San Juan County, Utah, and the Burro mine, San Miguel County, Colorado, USA. At both mines, it occurs as a low-temperature, secondary phase. The mineral is yellow to yellowish orange with pale yellow streak and fluoresces dull green yellow under 405 nm laser light. Crystals are transparent and have vitreous luster. It is brittle, with Mohs hardness of about 2½, splintery fracture, and three cleavages: {010} and {001} perfect, {100} good. The calculated density for the ideal formula is 4.433 g/cm^3. Crystals are acicular to bladed, elongate on [100], up to about 0.2 mm in length at the Blue Lizard, and up to 2 mm at the Burro. Ammoniozippeite is optically biaxial (+) with $\alpha = 1.678(2)$, $\beta = 1.724(3)$, $\gamma = 1.779(3)$ (white light); the measured $2V$ is 87.1(5)°; $r < v$ dispersion is weak; the optical orientation is $X = \mathbf{b}$, $Y = \mathbf{c}$, $Z = \mathbf{a}$; and pleochroism is X colorless, Y orange yellow, and Z yellow orange ($X \ll Y < Z$). Electron microprobe analyses (WDS mode) provided the empirical formulae $[(NH_4)_{1.97}Na_{0.03}]_{\Sigma 2.00}(U_{1.00}O_2)_2(S_{1.01}O_4)O_2\cdot H_2O$ and $[(NH_4)_{1.99}K_{0.06}Na_{0.04}]_{\Sigma 2.09}(U_{1.01}O_2)_2(S_{0.97}O_4)O_2\cdot H_2O$ for crystals from the Burro and Blue Lizard mines, respectively. The five strongest X-ray powder diffraction lines for Burro mine material are [d_{obs} Å(I)(hkl)]: 7.17(100)(020), 3.580(21)(040), 3.489(42)(203), 3.138(63)(223), and 1.6966(18)(229,426). Ammoniozippeite is orthorhombic, *Ccmb*, a 8.7944(3), b 14.3296(7), c 17.1718(12) Å, V 2164.0(2) Å^3, and $Z = 8$. The structure of ammoniozippeite ($R_1 = 0.0396$ for 932 reflections with $I_o > 2\sigma I$) contains edge-sharing zig-zag chains of pentagonal bipyramids that are linked by sharing corners with SO_4 groups, yielding a $[(UO_2)_2(SO_4)O_2]^{2-}$ sheet based on the zippeite-type topology. The interlayer region contains two NH_4^+ groups and one H_2O group *pfu*, statistically distributed over three sites.

Keywords: ammoniozippeite, new mineral, uranyl sulfate, crystal structure, zippeite-type topology, Blue Lizard mine, Utah, Burro mine, Colorado, USA.

[§] *Corresponding author e-mail address*: akampf@nhm.org

Introduction

In 1976, Frondel *et al*. examined the minerals of the zippeite group. They redefined the K-dominant phase as zippeite and defined sodium-zippeite, cobalt-zippeite, nickel-zippeite, magnesium-zippeite, and zinc-zippeite (now named natrozippeite, cobaltzippeite, nickelzippeite, magnesiozippeite, and zinczippeite). They also synthesized an NH_4-dominant zippeite. In 2003, Burns *et al*. conducted an in-depth crystal-chemical and structural investigation of eight synthetic phases with the zippeite structure, five with natural counterparts and three not known to occur in nature. Two of the latter were NH_4-dominant zippeites, $(NH_4)_4(H_2O)[(UO_2)_2(SO_4)O_2]_2$ and $(NH_4)_2[(UO_2)_2(SO_4)O_2]$, which they designated SZIPPNH$_4$I and SZIPPNH$_4$II, respectively. Herein we describe the mineral ammoniozippeite, a natural NH_4-dominant zippeite that corresponds closely to the SZIPPNH$_4$II phase synthesized and studied by Burns *et al*. (2003).

The name ammoniozippeite reflects the fact that this mineral is the ammonium analogue of zippeite, with NH_4^+ in place of K^+. The new mineral and name were approved by the Commission on New Minerals, Nomenclature and Classification (CNMNC) of the International Mineralogical Association (IMA2017-017). The description is based on one holotype specimen from the Burro mine, San Miguel County, Colorado, and one cotype specimen from the Blue Lizard mine, San Juan County, Utah. Both are deposited in the collections of the Natural History Museum of Los Angeles County, 900 Exposition Boulevard, Los Angeles, California 90007, USA, catalogue numbers 66625 (holotype) and 66626 (cotype). It should be noted that the zippeite group has not yet been formally approved by the CNMNC.

Occurrence

Ammoniozippeite was first collected underground in the Blue Lizard mine, Red Canyon, White Canyon mining district, San Juan County, Utah (37°33′26″N 110°17′44″W). Larger and better crystals were subsequently collected underground at the Burro mine, Slick Rock district, San Miguel County, Colorado, USA (38°2′42″N 108°53′23″W). Other non-type localities at which we have verified the occurrence of ammoniozippeite include the Green Lizard, Markey, and Giveaway-Simplot mines (near the Blue Lizard mine) in Red Canyon.

The Blue Lizard mine is located about 72 km west of the town of Blanding, Utah, and about 22 km southeast of Good Hope Bay on Lake Powell. Mineralized channels are in the Shinarump member of the Chinle Formation. The Shinarump member consists of medium- to coarse-grained sandstone, conglomeratic sandstone beds, and thick siltstone lenses. Ore minerals were deposited as replacements of wood and other organic material and as disseminations in the enclosing sandstone (Chenoweth 1993). Since the mine closed in 1978, oxidation of primary ores in the humid underground environment has produced a variety of secondary minerals, mainly sulfates, occurring as efflorescent crusts on the surfaces of mine walls (Kampf *et al*. 2015).

The Burro mine is located near the southern end of the Uravan Mineral Belt, in which uranium and vanadium minerals occur together in bedded or roll-front deposits in sandstone of the Salt Wash member of the Jurassic Morrison Formation (Carter & Gualtieri 1965, Shawe 2011). The uranium and vanadium ore mineralization was deposited where solutions rich in U and V encountered pockets of strongly reducing solutions that had developed around accumulations of carbonaceous plant material. Mining operations have exposed both unoxidized and oxidized U and V phases. Under ambient temperatures and generally oxidizing near-surface conditions, water reacts with pyrite to form aqueous solutions with relatively low pH, which then react with the earlier-formed phases, resulting in diverse suites of secondary minerals. At both the Blue Lizard and Burro mines the NH_4^+ presumably derives from organic matter in the deposit.

Ammoniozippeite is rare at the Burro mine, where it occurs on a matrix consisting of asphaltum, quartz, and calcite, and is associated with gypsum, natrojarosite, and natrozippeite. At the Blue Lizard mine it is more widespread, usually occurring on a matrix made up mostly of partially recrystallized quartz grains, which are remnants of the original sandstone. At the Blue Lizard mine ammoniozippeite has been found with a wide variety of other secondary phases including blödite, bobcookite, brochantite, chalcanthite, devilline, dickite, ferrinatrite, gerhardtite, gypsum, johannite, krönkite, magnesiozippeite, natrozippeite, pentahydrate, pickeringite, plášilite, posnjakite, redcanyonite, wetherillite, and other potentially new uranyl sulfate minerals, currently under study.

Physical and Optical Properties

Ammoniozippeite crystals are acicular to bladed, usually tapering to a point at the Blue Lizard mine, but occasionally with rectangular (square) terminations, particularly at the Burro mine. Crystals from the Blue Lizard mine rarely exceed 0.2 mm in length, but a remarkable occurrence at the Burro mine has provided crystals up to about 2 mm in length (Fig. 1). Blades are elongated on [100]; those from the Burro mine are

FIG. 1. Ammoniozippeite blades up to about 2 mm long on asphaltum from the Burro mine. Note that some of the blades exhibit square terminations {100}. The field of view is 2.5 mm.

flattened on {001}, while those from the Blue Lizard mine are flattened on {010}. The blades from the Burro mine have simple rectangular morphology, only exhibiting the forms {001}, {010}, and {100}. Short blades at the Blue Lizard mine are lozenge-shaped (Fig. 2), exhibiting the prism forms {001} and {010}, with spear-like terminations that often appear rounded and are presumably composed of various combinations of {101}, {102}, {103}, and {104} (Fig. 3). Although zippeite-structure-type minerals often exhibit twinning, ammoniozippeite crystals on the type specimens only very rarely appear to exhibit twinning when examined under crossed polarizers. No twinning was noted by XRD.

The mineral is yellow to yellowish orange with pale yellow streak and fluoresces dull green yellow under 405 nm laser light. Crystals are transparent and have vitreous luster. The mineral is brittle, with Mohs hardness of about 2½ based on scratch tests. The fracture is splintery and there are three cleavages: {010} and {001} perfect, {100} good.

The density could not be measured because it is greater than floatation liquids and there is insufficient material for physical measurement. The calculated

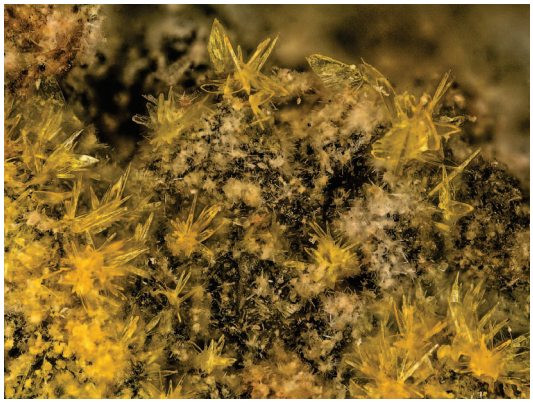

FIG. 2. Lozenge-shaped ammoniozippeite blades from the Blue Lizard mine. The field of view is 1.7 mm.

densities for the empirical formulae are 4.427 and 4.470 g/cm^3 for Burro mine and Blue Lizard mine material, respectively. The calculated density for the ideal formula is 4.433 g/cm^3.

The optical properties were determined in white light for Burro mine crystals. Ammoniozippeite is optically biaxial (+) with $\alpha = 1.678(2)$, $\beta = 1.724(3)$, $\gamma = 1.779(3)$. The $2V$ measured using extinction data analyzed with EXCALIBRW (Gunter *et al*. 2004) is

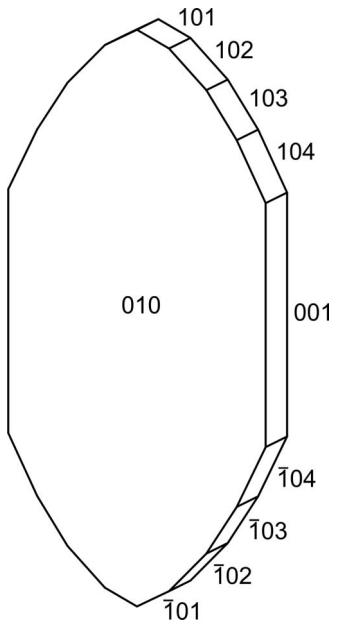

FIG. 3. Crystal drawing of a lozenge-shaped ammoniozippeite crystal; the clinographic projection is in non-standard orientation, **a** vertical.

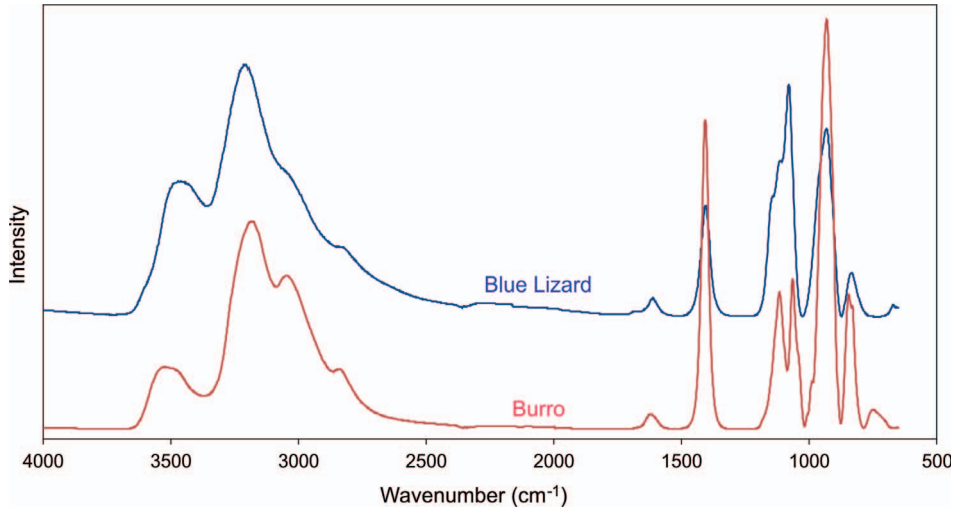

FIG. 4. Infrared spectra of ammoniozippeite from the Burro and Blue Lizard mines, collected from 4000 to 650 cm^{-1}.

87.1(5)°; the calculated $2V$ is 87.4°. The dispersion is weak, $r < v$. The optical orientation is $X = \mathbf{b}$, $Y = \mathbf{c}$, $Z = \mathbf{a}$. The pleochroism is X colorless, Y orange yellow, and Z yellow orange; $X \ll Y < Z$.

The mineral is insoluble in room-temperature H_2O and exhibits hydrophobic behavior. It is very rapidly soluble in room-temperature dilute HCl.

Infrared Spectroscopy

Attenuated total reflectance (ATR) Fourier transform infrared (FTIR) spectra were obtained using a liquid N_2-cooled SENSIR Technologies IlluminatIR instrument mounted on an Olympus BX51 microscope. An ATR objective was pressed into crystals of ammoniozippeite and measured from 4000 to 650 cm^{-1}. The infrared spectra of ammoniozippeite from the Burro and Blue Lizard mines are very similar (Fig. 4). Mode assignments for material from the Burro mine given below are primarily based on those of Čejka (1999). Several intense, broad bands observed between ~3500 and ~2800 cm^{-1} are attributed to stretching vibrations (ν O–H) of hydrogen-bonded water molecules, along with N–H stretching vibrations from interlayer NH_4^+ molecules. Calculated O–H···O hydrogen donor–acceptor distances are in the range ~2.9–2.6 Å, using the correlation function given by Libowitzky (1999). A weak band found at 1626 cm^{-1} is assigned as the ν_2 (δ)-bending vibration of hydrogen-bonded crystalline water. A medium-strong band at 1408 cm^{-1} is assigned to the N–H bending vibration of NH_4^+ molecules (Pekov *et al*. 2014). Absorption bands at 1120 (shoulder at 1138) and 1065 cm^{-1} are assigned to the split triply degenerate ν_3 SO_4^{2-} antisymmetric stretching vibration. Weak bands attributed to the ν_1 SO_4^{2-} symmetric stretch occur at 1008 and 993 cm^{-1}. A relatively broad and strong band at 933 cm^{-1} is assigned to the antisymmetric ν_3 UO_2^{2+} stretching vibration. A two-component band at 846 and 832 cm^{-1} is attributed to the ν_1 UO_2^{2+} symmetric stretch, which, although forbidden by selection rules, may be observed due to a slight deviation in the linearity of the uranyl bond. Coincidences with the libration mode of H_2O molecules are also possible around 830 cm^{-1}. Calculated uranyl U–O bond lengths using the empirical relation given by Bartlett & Cooney (1989) are 1.77 Å (ν_3) and 1.78 Å (ν_1).

Raman Spectroscopy

Raman spectroscopy was conducted using a Horiba XploRA PLUS instrument. Pronounced fluorescence was observed using a 532 nm diode laser; consequently, a 785 nm diode laser was utilized. The spectrum, recorded from 1600 to 100 cm^{-1}, is shown in Figure 5. A weak and rather broad band centered at approximately 1390 cm^{-1} is related to the ν_2 (δ) H–N–H bending vibration of NH_4^+ cations. The split triply degenerate ν_3 SO_4^{2-} antisymmetric stretching vibrations occur as very weak bands centered at 1098 cm^{-1}, with a shoulder at ~1120 cm^{-1}. A low-intensity band at 1013 cm^{-1} is assigned to the ν_1 SO_4^{2-} symmetric stretching vibration. The ν_1 UO_2^{2+} symmetric stretching vibration is present as a very intense band at 826 cm^{-1}, with shoulders at 848 and 806 cm^{-1} (which may be artefacts). Bartlett & Cooney (1989) provide an empirical relation to derive the approximate $U–O_{yl}$ bond lengths from the band positions assigned to the

TABLE 1. CHEMICAL COMPOSITION (wt.%) FOR AMMONIOZIPPEITE

	Burro mine (five analyses based on four crystals)			Blue Lizard mine (four analyses based on three crystals)			Probe
Const.	Mean	Range	SD	Mean	Range	SD	standard
$(NH_4)_2O$	7.29	6.96–7.76	0.31	7.36	6.88–7.64	0.33	syn. Cr_2N
Na_2O	0.13	0.04–0.14	0.06	0.19	0.05–0.33	0.11	albite
K_2O	–	–	–	0.43	0.36–0.51	0.08	sanidine
SO_3	11.45	10.80–12.44	0.64	11.00	10.61–11.37	0.35	baryte
UO_3	81.10	79.24–84.24	2.02	81.90	79.69–85.04	2.25	syn. UO_2
H_2O*	2.56			2.56			
Total	102.53			103.44			

* Based on the crystal structure

UO_2^{2+} stretching vibrations, which gives 1.784 Å (826 cm^{-1}), in excellent agreement with the U–O_{yl} bond length measured from the X-ray data, 1.782 Å. Very weak bands at 664 and 608 cm^{-1} are attributed to the split triply degenerate ν_4 (δ) SO_4^{2-} bending vibrations and bands at 508 (w), 461 (m), and 406 (s) cm^{-1} are attributed to the split doubly degenerate ν_2 (δ) SO_4^{2-} bending vibrations. Composite bands at 368 and 327 cm^{-1} are attributed to ν (U–$O_{equatorial}$) stretching vibrations, but may also coincide with the $\nu_{rotational}$ of interlayer NH_4^+ (Heyns *et al*. 1987). A band at 283 cm^{-1} (with a weak shoulder at ~268 cm^{-1}) may also arise from such NH_4^+ modes. Two overlapping medium-intensity bands at 213 and 203 cm^{-1} are assigned to ν_2 (δ) U–O–U bending or U–O_{eq}–ligand stretching modes (*cf*. Bullock & Parret 1970, Ohwada 1976, Brittain *et al*. 1985, Plášil *et al*. 2010). The remaining strong band at 148 cm^{-1} is assigned to external lattice vibration modes and UO_2^{2+} translations and rotations (Plášil *et al*. 2010).

Chemical Composition

Chemical analyses were performed at the University of Utah using a Cameca SX-50 electron microprobe with four wavelength-dispersive spectrometers and *Probe for EPMA* software. Analytical conditions were 15 kV accelerating voltage, 10 nA beam current, and a beam diameter of 5 μm. Counting times were 30 s on peak and 30 s on background for

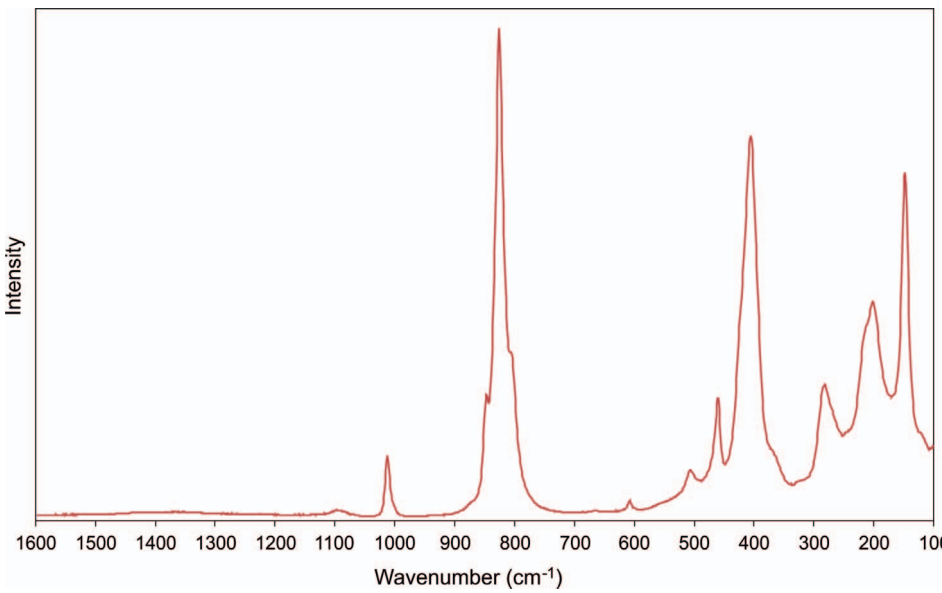

FIG. 5. Raman spectrum of ammoniozippeite from the Burro mine recorded using a 785 nm diode laser, collected from 1600 to 100 cm^{-1}.

TABLE 2. POWDER X-RAY DATA (*d* IN Å) FOR AMMONIOZIPPEITE FROM THE BURRO MINE

I_{obs}	d_{obs}	d_{calc}	I_{calc}	*hkl*
7	8.64	8.5859	15	0 0 2
100	7.17	7.1648	100	0 2 0
		6.8695	2	1 1 1
		5.6465	1	1 1 2
10	5.503	5.5010	8	0 2 2
13	4.270	4.2930	5	0 0 4
		4.2598	9	2 0 1
4	4.090	4.0773	4	1 3 1
4	3.761	3.7709	3	1 3 2
14	3.670	3.6825	6	0 2 4
		3.6615	8	2 2 1
21	3.580	3.5824	16	0 4 0
42	3.489	3.4870	34	2 0 3
3	3.308	3.3062	3	0 4 2
63	3.138	3.1354	53	2 2 3
1	3.003	3.0012	1	1 3 4
6	2.861	2.8620	12	0 0 6
		2.7505	1	0 4 4
4	2.733	2.7417	2	2 4 1
		2.7066	1	2 0 5
		2.6912	2	1 5 1
10	2.665	2.6578	12	0 2 6
3	2.608	2.5972	3	1 5 2
		2.5320	1	2 2 5
13	2.502	2.4987	12	2 4 3
3	2.393	2.3883	3	0 6 0
3	2.302	2.3009	3	0 6 2
6	2.237	2.2360	8	0 4 6
9	2.199	2.1986	6	4 0 0
		2.1594	2	3 3 4
11	2.141	2.1465	1	0 0 8
		2.1423	4	2 0 7
		2.1346	1	1 5 5
		2.1299	3	4 0 2
		2.1179	1	1 3 7
12	2.1005	2.1019	7	4 2 0
		2.0870	1	0 6 4
		2.0832	1	2 6 1
12	2.0479	2.0562	1	0 2 8
		2.0525	5	2 2 7
		2.0416	3	4 2 2
		2.0349	1	3 5 1
		2.0204	1	3 3 5
		1.9933	1	3 5 2
		1.9805	3	1 7 1
11	1.9769	1.9704	8	2 6 3
6	1.9494	1.9569	2	4 0 4
		1.9421	3	1 7 2
		1.9111	1	1 3 8
8	1.8801	1.8877	2	4 2 4
		1.8738	5	4 4 0
9	1.8354	1.8494	1	3 5 4
		1.8386	2	2 4 7
		1.8337	3	0 6 6
		1.8308	1	4 4 2
		1.8231	1	1 5 7
		1.8083	1	1 7 4
		1.7912	2	0 8 0
14	1.7505	1.7598	2	3 5 5
		1.7534	1	0 8 2
		1.7503	4	2 0 9
		1.7435	6	4 0 6
6	1.7206	1.7243	2	1 7 5
		1.7174	2	4 4 4
18	1.6966	1.7003	8	2 2 9
		1.6941	7	4 2 6
		1.6862	1	1 5 8
4	1.6594	1.6699	3	0 2 10
		1.6512	1	2 8 1
		1.6472	1	3 7 2
3	1.6222	1.6175	2	4 6 0
4	1.5937	1.5947	1	2 6 7
		1.5933	2	2 8 3
		1.5896	1	4 6 2
13	1.5691	1.5726	5	2 4 9
		1.5677	5	4 4 6
		1.5631	1	3 7 4
		1.5602	1	1 9 1
3	1.5440	1.5485	1	0 4 10
		1.5472	1	1 7 7
		1.5413	2	1 9 2
3	1.5119	1.5183	2	0 8 6
		1.5079	1	3 7 5
		1.4718	1	1 9 4
		1.4608	2	1 7 8
5	1.4262	1.4310	2	6 2 1
		1.4254	1	1 9 5
		1.4199	2	6 0 3
7	1.4097	1.4118	4	2 6 9
		1.4082	2	4 6 6
		1.4033	1	0 2 12
7	1.3910	1.3945	1	3 9 1
		1.3928	3	6 2 3
		1.3887	1	4 8 0
		1.3809	1	3 9 2
		1.3742	1	2 8 7
		1.3545	1	1 5 11
6	1.3247	1.3303	1	3 9 4
		1.3298	1	4 2 10
		1.3289	1	0 4 12
		1.3254	1	2 10 3
		1.3222	1	3 7 8
		1.3200	3	6 4 3
		1.3183	1	5 7 2

each element. Raw X-ray intensities were corrected for matrix effects with a $\phi\rho(z)$ algorithm (Pouchou & Pichoir 1991). Time-dependent intensity corrections were applied to N, U, and S, and the N concentration was corrected for the partial overlap of the U N4-N6 emission line on the N *K*α peak. Because insufficient material was available for a direct determination of H_2O, it was calculated based upon the structure determination. Infrared spectroscopy confirmed the presence of H_2O. The high totals could be the result of loss of loosely held H_2O under vacuum or from beam damage during the analyses. The sample exhibited visible beam damage. The results are given in Table 1.

The empirical formulae (calculated on the basis of 11 O atoms per formula unit, *apfu*) are $[(NH_4)_{1.97}Na_{0.03}]_{\Sigma 2.00}(U_{1.00}O_2)_2(S_{1.01}O_4)O_2{\cdot}H_2O$ for the Burro mine and $[(NH_4)_{1.99}K_{0.06}Na_{0.04}]_{\Sigma 2.09}(U_{1.01}O_2)_2(S_{0.97}O_4)O_2{\cdot}H_2O$ for the Blue Lizard mine. The ideal formula is $(NH_4)_2[(UO_2)_2$

TABLE 3. DATA COLLECTION AND STRUCTURE REFINEMENT DETAILS FOR AMMONIOZIPPEITE

Diffractometer	Rigaku R-Axis Rapid II
X-ray radiation/power	Mo$K\alpha$ ($\lambda = 0.71075$ Å)/50 kV, 40 mA
Temperature	293(2) K
Structural Formula	$(NH_4)_2[(UO_2)_2(SO_4)O_2]\cdot H_2O$
Space group	*Ccmb*
Unit cell dimensions	$a = 8.7944(3)$ Å
	$b = 14.3296(7)$ Å
	$c = 17.1718(12)$ Å
V	2164.0(2)Å^3
Z	8
Density (for above formula)	4.384 g/cm
Absorption coefficient	30.141 mm^{-1}
F(000)	2432
Crystal size	130 × 50 × 15 μm
θ range	3.61 to 27.46°
Index ranges	$-11 \le h \le 9$, $-17 \le k \le 18$, $-22 \le l \le 22$
Reflections collected/unique	10176/1249; $R_{int} = 0.048$
Reflections with $I > 2\sigma I$	923
Completeness to $\theta = 27.46°$	97.2%
Refinement method	Full-matrix least-squares on F^2
Parameter/restraints	69/0
GoF	1.094
Final R indices ($I > 2\sigma I$)	$R_1 = 0.0396$, $wR_2 = 0.0924$
R indices (all data)	$R_1 = 0.0559$, $wR_2 = 0.1022$
Largest diff. peak/hole	+3.91/–1.79 e Å^{-3}

$R_{int} = \Sigma|F_o^2 - F_o^2(\text{mean})|/\Sigma[F_o^2]$. GoF $= S = \{\Sigma[w(F_o^2 - F_c^2)^2]/(n-p)\}^{1/2}$. $R_1 = \Sigma||F_o| - |F_c||/\Sigma|F_o|$. $wR_2 = \{\Sigma[w(F_o^2 - F_c^2)^2]/\Sigma[w(F_o^2)^2]\}^{1/2}$; $w = 1/[\sigma^2(F_o^2) + (aP)^2 + bP]$ where a is 0.0373, b is 160.4774, and P is $[2F_c^2 + \text{Max}(F_o^2, 0)]/3$.

TABLE 4. ATOM COORDINATES AND DISPLACEMENT PARAMETERS (Å^2) FOR AMMONIOZIPPEITE

	x/a	y/b	z/c	U_{eq}		
U	0.12645(5)	0.23208(3)	0.58657(2)	0.01678(18)		
S	0.3750(5)	0.25	0.75	0.0181(8)		
O1	0.3740(9)	0.2435(9)	0.5441(5)	0.039(3)		
O2	0.4683(10)	0.3097(7)	0.6995(5)	0.025(2)		
O3	0.2799(9)	0.1880(7)	0.7009(5)	0.024(2)		
O4	0.1239(10)	0.1098(8)	0.5690(6)	0.033(2)		
O5	0.1313(12)	0.3521(7)	0.6144(6)	0.034(2)		
N1	0.139(3)	0	0.7484(17)	0.093(9)		
N2	–0.149(3)	0	0.5964(16)	0.086(9)		
N3	0.412(5)	0	0.561(2)	0.135(14)		
	U^{11}	U^{22}	U^{33}	U^{23}	U^{13}	U^{12}
U	0.0163(3)	0.0251(3)	0.0090(2)	–0.00016(16)	–0.00009(18)	0.00197(19)
S	0.0092(18)	0.034(2)	0.0108(18)	–0.0004(15)	0	0
O1	0.003(4)	0.100(9)	0.012(4)	0.000(5)	–0.004(3)	–0.008(5)
O2	0.017(5)	0.035(6)	0.024(5)	–0.004(4)	0.007(3)	–0.002(4)
O3	0.019(5)	0.040(6)	0.014(4)	–0.001(4)	–0.004(3)	–0.005(4)
O4	0.016(5)	0.045(6)	0.037(5)	–0.016(4)	–0.009(4)	0.007(4)
O5	0.046(6)	0.024(5)	0.031(5)	0.004(4)	–0.001(5)	0.001(5)

TABLE 5. SELECTED BOND DISTANCES (Å) FOR AMMONIOZIPPEITE*

U–O4	1.778(11)	S–O2 (×2)	1.469(9)	N2–O5 (×2)	2.88(2)	N3–OW3	2.59(8)
U–O5	1.786(10)	S–O3 (×2)	1.483(9)	N2–O4 (×2)	2.91(3)	N3–O4 (×2)	2.99(4)
U–O1	2.271(9)	<S–O>	1.476	N2–O4 (×2)	3.25(3)	N3–O5 (×2)	3.01(3)
U–O1	2.302(8)			N2–OW1	3.25(4)	N3–O1 (×2)	3.52(1)
U–O1	2.363(8)	N1–O3 (×2)	3.08(2)	N2–O2 (×2)	3.41(2)	N3–OW2	3.55(5)
U–O2	2.460(8)	N1–O5 (×2)	3.17(2)	N2–OW3	3.55(5)	<N3–O>	3.148
U–O3	2.465(8)	N1–O2 (×2)	3.22(2)	<N2–O>	3.170		
$<U–O_{UR}>$	1.782	N1–OW2	3.25(4)				
$<U–O_{EQ}>$	2.372	N1–O4 (×2)	3.46(3)				
		<N1–O>	3.234				

* N1, N2, and N3 sites acting as O (H_2O sites) are labeled OW1, OW2, and OW3, respectively.

$(SO_4)O_2]\cdot H_2O$, which requires $(NH_4)_2O$ 7.21, SO_3 11.09, UO_3 79.21, and H_2O 2.49, total 100.00 wt.%.

Gladstone-Dale Compatibility

The specific refractive energy for UO_3, $k(UO_3)$, was given by Larsen & Berman (1934) as 0.134. The value was revised to 0.118 by Mandarino (1976). Piret & Deliens (1989) found that the original value of 0.134 worked best for uranyl phosphates and arsenates, but they did not address other uranyl compounds. We have found that the value of 0.118 from Mandarino (1976) usually works well for uranyl sulfates; however, there are exceptions. It is likely that the degree of condensation of uranyl polyhedra impacts the specific refractive energy. A more detailed study is certainly in order. For ammoniozippeite from the Burro mine, the Gladstone-Dale compatibility, $1 - (K_p/K_c)$, is –0.052 (good compatibility) using $k(UO_3) = 0.118$, and 0.027 (excellent compatibility) using $k(UO_3) = 0.134$. A $k(UO_3)$ value intermediate between 0.118 and 0.134 would provide the best compatibility for ammoniozippeite.

X-Ray Diffraction: Experimental

Powder X-ray studies were done using a Rigaku R-Axis Rapid II curved imaging plate microdiffractometer with monochromatized Mo$K\alpha$ radiation (λ = 0.71075 Å). A Gandolfi-like motion on the φ and ω axes was used to randomize the samples. X-ray powder diffraction patterns for ammoniozippeite from the Burro and Blue Lizard mines are very similar. Observed d values and intensities for Burro mine ammoniozippeite were derived by profile fitting using JADE 2010 software. Data are given in Table 2. Unit-cell parameters refined from the powder data using JADE 2010 with whole-pattern fitting are a 8.812(3), b 14.351(5), c 17.204(5) Å, and $V = 2175.6(12)$ Å^3.

Single-crystal data were collected using the same diffractometer and radiation as noted above. The Rigaku CrystalClear software package was used for processing the structure data, including the application of an empirical absorption correction using the multi-scan method with ABSCOR (Higashi 2001). An initial structure model with most atoms located was obtained by the charge-flipping method using SHELXT

TABLE 6. BOND-VALENCE ANALYSIS FOR AMMONIOZIPPEITE (VALUES ARE EXPRESSED IN VALENCE UNITS*)

	U	S	N1	N2	N3	Σ
O1	0.62, 0.58, 0.51				$^{\times2\downarrow}0.03^{\times\frac{2}{3}\rightarrow}$	1.73
O2	0.42	$1.51^{\times2\downarrow}$	$^{\times2\downarrow}0.07^{\times\frac{2}{3}\rightarrow}$	$^{\times2\downarrow}0.04^{\times\frac{2}{3}\rightarrow}$		2.01
O3	0.41	$1.46^{\times2\downarrow}$	$^{\times2\downarrow}0.10^{\times\frac{2}{3}\rightarrow}$			1.94
O4	1.76		$^{\times2\downarrow}0.04^{\times\frac{2}{3}\rightarrow}$	$^{\times2\downarrow}0.16^{\times\frac{2}{3}\rightarrow}$, $^{\times2\downarrow}0.06^{\times\frac{2}{3}\rightarrow}$	$^{\times2\downarrow}0.13^{\times\frac{2}{3}\rightarrow}$	2.00
O5	1.73		$^{\times2\downarrow}0.08^{\times\frac{2}{3}\rightarrow}$	$^{\times2\downarrow}0.17^{\times\frac{2}{3}\rightarrow}$	$^{\times2\downarrow}0.12^{\times\frac{2}{3}\rightarrow}$	1.97
OW1				0.06		0.06
OW2			0.06		0.03	0.09
OW3				0.03	0.37	0.40
Σ	6.04	5.94	0.64	0.95	0.96	

* Multiplicity is indicated by $\times\rightarrow\downarrow$. NH_4^+–O bond-valence parameters from García-Rodríguez *et al.* (2000). U^{6+}–O and S^{6+}–O bond-valence parameters are from Gagné & Hawthorne (2015). Hydrogen-bond contributions are not included.

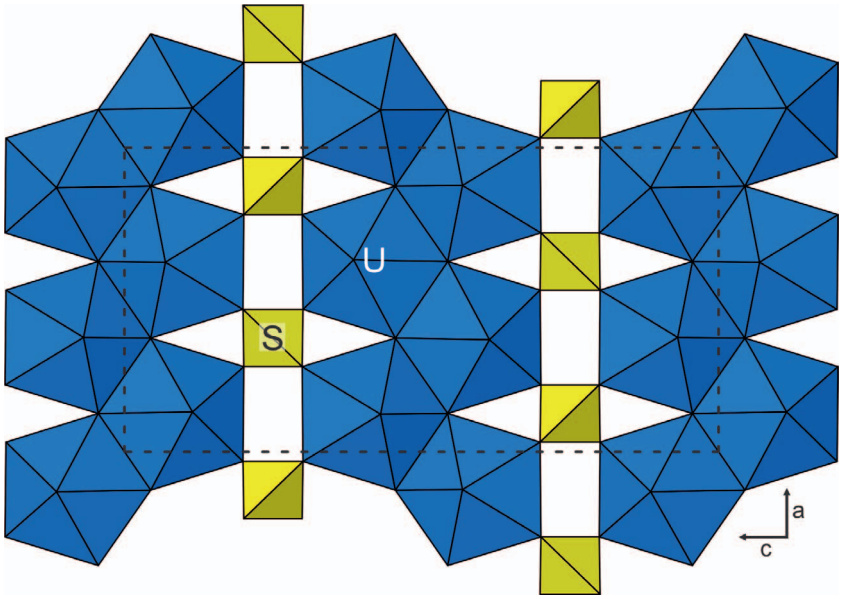

FIG. 6. The uranyl-sulfate sheet in the structure of ammoniozippeite. The unit-cell outline is shown by dashed lines.

(Sheldrick 2015a). SHELXL-2016 (Sheldrick 2015b) was used for the refinement of the structure. Difference-Fourier syntheses located all non-hydrogen atoms not located in the original structure solution, but hydrogen atom sites could not be resolved. The structure was found to be identical to that of the synthetic orthorhombic NH_4 analogue of zippeite (SZIPPNH4II; Burns *et al*. 2003), except that we found one additional interlayer site. The three interlayer sites (NH_4 or H_2O) exhibited high isotropic displacement parameters. Efforts to refine these sites anisotropically suggested splitting of the sites; however, efforts to resolve the split sites were only marginally successful. Ultimately, we decided to report the unsplit sites with isotropic displacement parameters. Furthermore, in line with the results of the EPMA and considering the coordination environments of the sites, we have assumed each to be statistically occupied by 2/3 N (NH_4) and 1/3 O (H_2O). In so doing, all three sites refined to near or slightly above full occupancy. Four of the eight highest residuals (3.94, 2.35, 2.27, and 2.01 e Å $^{-3}$) are less than 1 Å from the U site and presumably result from an imperfect absorption correction. The other four high residuals (2.31, 2.31, 1.89, and 1.71 e Å^{-3}) are nearest to N sites (from 0.76 to 2.12 Å) and could be related to the disorder in the interlayer and/or the aforementioned site splitting.

Data collection and refinement details are given in Table 3, atom coordinates and displacement parameters in Table 4, selected bond distances in Table 5, and a bond-valence analysis in Table 6. A CIF file containing observed and calculated structure factors has been deposited and is available from the Depository of Unpublished Data on the MAC website [document Burroite CM56_10.3749/canmin.1800002]. Note that Burns *et al*. (2003) reported the structure in the space group *Cmca*; however, to be consistent with the cells of the monoclinic zippeite-group minerals, we report the structure in the non-standard space group *Ccmb*.

ATOMIC ARRANGEMENT OF AMMONIOZIPPEITE

The U sites in the structure of ammoniozippeite are surrounded by seven O atoms forming a squat UO_7 pentagonal bipyramid. This is the most typical coordination for U^{6+}, particularly in uranyl sulfates, where the two short apical bonds of the bipyramid constitute the UO_2^{2+} uranyl group. In the structure of ammoniozippeite, pentagonal bipyramids link by sharing edges to form zig-zag chains two bipyramids wide along [100]. The chains are linked by sharing corners with SO_4 tetrahedra. Each sulfate tetrahedron links four different bipyramids (two bipyramids in each of two adjacent chains) and propagates the zippeite-type sheet along [001], yielding a $[(UO_2)_2(SO_4)O_2]^{2-}$ sheet parallel to {010} (Fig. 6). This sheet has the extensively studied zippeite-type topology, as designated by the hierarchy of Burns (2005) and Lussier *et al*. (2016). The interlayer region in the ammoniozippeite structure contains two NH_4^+ groups

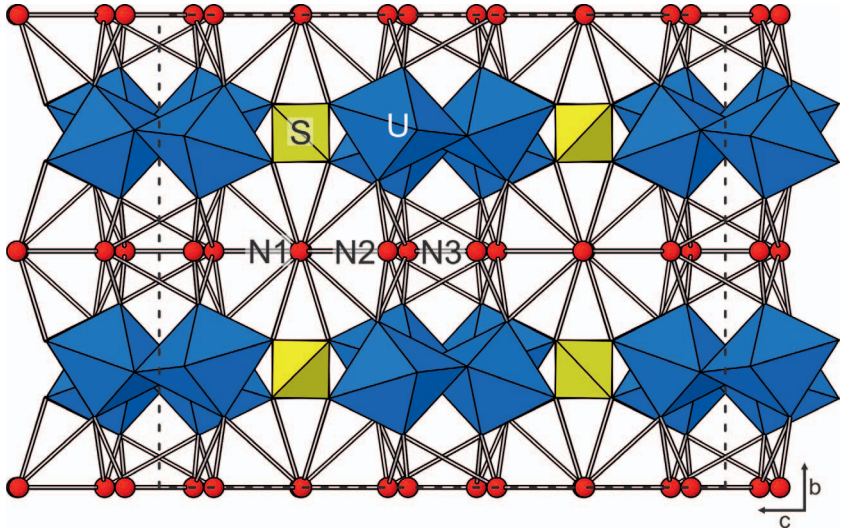

FIG. 7. The structure of ammoniozippeite viewed down **a**, the chain direction. NH_4–O bonds are shown as sticks. The unit-cell outline is shown by dashed lines.

and one H_2O group *pfu*, statistically distributed over three sites (N1, N2, and N3). By contrast, Burns *et al.* (2003) reported that their orthorhombic NH_4 zippeite (SZIPPNH$_4$II) contained two fully occupied N sites and no H_2O in the interlayer. The N1 and N2 sites in ammoniozippeite correspond to the N1 and N2 sites in SZIPPNH$_4$II, while the N3 site in ammoniozippeite represents an additional interlayer site.

Considering adjacent N sites as H_2O groups, the NH_4^+ groups coordinate to eight, nine, or ten O sites between distances of 2.59 and 3.55 Å. Note that we have elected to include the very long N–O distances because of the positional disorder indicated by the large isotropic displacement parameters of the N sites. The entire structure is shown in Figure 7.

ACKNOWLEDGMENTS

An anonymous reviewer and Giovanni Ferraris are thanked for their constructive comments on the manuscript. A portion of this study was funded by the John Jago Trelawney Endowment to the Mineral Sciences Department of the Natural History Museum of Los Angeles County. JP acknowledges support from the Ministry of Education, Youth and Sports National sustainability programme I of the Czech Republic (Project No. LO1603). BPN thanks the Northern California Mineralogical Association for partial support for electron microprobe analyses of new minerals from the Colorado Plateau. We would like to thank Don Coram, the owner of the Burro mine, for allowing us access to the property, and to Okie Howell and Jess Fulbright for providing logistical support during our visits.

REFERENCES CITED

BARTLETT, J.R. & COONEY, R.P. (1989) On the determination of uranium-oxygen bond lengths in dioxouranium(VI) compounds by Raman spectroscopy. *Journal of Molecular Structure* **193**, 295–300.

BRITTAIN, H.G., ANSARI, P., TOIVONEN, J., NIINISTO, L., TSAO, L., & PERRY, D.L. (1985) Photophysical studies of uranyl complexes. VIII. Luminescence spectra of $UO_2SO_4{\cdot}3\frac{1}{2}H_2O$ and two polymorphs of bis(urea) uranyl sulfate. *Journal of Solid State Chemistry* **59**, 259–264.

BULLOCK, H. & PARRET, F.W. (1970) The low frequency infrared and Raman spectroscopic studies of some uranyl complexes: the deformation frequency of the uranyl ion. *Canadian Journal of Chemistry* **48**, 3095–3097.

BURNS, P.C. (2005) U^{6+} minerals and inorganic compounds: insights into an expanded structural hierarchy of crystal structures. *Canadian Mineralogist* **43**, 1839–1894.

BURNS, P.C., DEELY, K.M., & HAYDEN, L.A. (2003) The crystal chemistry of the zippeite group. *Canadian Mineralogist* **41**, 687–706.

CARTER, W.D. & GUALTIERI, J.L. (1965) Geology and uranium-vanadium deposits of the La Sal quadrangle, San Juan County, Utah and Montrose County, Colorado. *United States Geological Survey Professional Paper* **508**.

ČEJKA J. (1999) Infrared and thermal analysis of the uranyl minerals. *Reviews in Mineralogy* **38**, 521–622.

CHENOWETH, W.L. (1993) The geology and production history of the uranium deposits in the White Canyon mining district, San Juan County, Utah. *Utah Geological Survey Miscellaneous Publication* **93(3)**, 26 pp.

FRONDEL, C., ITO, J., HONEA, R.M., & WEEKS, A.M. (1976) Mineralogy of the zippeite group. *Canadian Mineralogist* **14**, 429–436.

GAGNÉ, O.C. & HAWTHORNE, F.C. (2015) Comprehensive derivation of bond-valence parameters for ion pairs involving oxygen. *Acta Crystallographica* **B71**, 562–578.

GARCÍA-RODRÍGUEZ, L., RUTE-PÉREZ, Á., PIÑERO, J.R., & GONZÁLEZ-SILGO, C. (2000) Bond-valence parameters for ammonium-anion interactions. *Acta Crystallographica* **B56**, 565–569.

GUNTER, M.E., BANDLI, B.R., BLOSS, F.D., EVANS, S.H., SU, S.C., & WEAVER, R. (2004) Results from a McCrone spindle stage short course, a new version of EXCALIBR and how to build a spindle stage. *The Microscope* **52**, 23–39.

HEYNS, A.M., VENTER, M.W., & RANGE, K.-J. (1987) The vibrational spectra of NH_4VO_3 at elevated temperatures and pressures. *Zeitschrift für Naturforshung* **42b**, 843–852.

HIGASHI, T. (2001) *ABSCOR*. Rigaku Corporation, Tokyo, Japan.

KAMPF, A.R., KASATKIN, A.V., ČEJKA, J., & MARTY, J. (2015) Plášilite, $Na(UO_2)(SO_4)(OH)\cdot 2H_2O$, a new uranyl sulfate mineral from the Blue Lizard mine, San Juan County, Utah, USA. *Journal of Geosciences* **60**, 1–10.

LARSEN, E.S. & BERMAN, H. (1934) The microscopic determination of the nonopaque minerals. *United States Geological Survey Bulletin* **848**.

LIBOWITZKY, E. (1999) Correlation of O–H stretching frequencies and O–H···O hydrogen bond lengths in minerals. *Monatshefte für Chemie* **130**, 1047–1059.

LUSSIER, A.J., BURNS, P.C., & KING-LOPEZ, R. (2016) A revised and expanded structure hierarchy of natural and synthetic hexavalent uranium compounds. *Canadian Mineralogist* **54**, 177–283.

MANDARINO, J.A. (1976) The Gladstone-Dale relationship — Part 1: Derivation of new constants. *Canadian Mineralogist* **14**, 498–502.

OHWADA, K. (1976) Infrared spectroscopic studies of some uranyl nitrate complexes. *Journal of Coordination Chemistry* **6**, 75–80.

PEKOV, I.V., KRIVOVICHEV, S.V., YAPASKURT, V.O., CHUKANOV, N.V., & BELAKOVSKIY, D.I. (2014) Beshtauite, $(NH_4)_2(UO_2)(SO_4)_2\cdot 2H_2O$, a new mineral from Mount Beshtau, Northern Caucasus, Russia. *American Mineralogist* **99**, 1783–1787.

PIRET, P. & DELIENS, M. (1989) The Gladstone-Dale constant $k(UO_3)$ for uranyl phosphates and arsenates. *Canadian Mineralogist* **27**, 533–534.

PLÁŠIL, J., BUIXADERAS, E., ČEJKA, J., SEJKORA, J., JEHLIČKA, J., & NOVÁK, M. (2010) Raman spectroscopic study of the uranyl sulphate mineral zippeite: low wavenumber and U–O stretching regions. *Analytical and Bioanalytical Chemistry* **397**, 2703–2715.

POUCHOU, J.-L. & PICHOIR, F. (1991) Quantitative analysis of homogeneous or stratified microvolumes applying the model "PAP." *In* Electron Probe Quantitation (K.F.J. Heinrich & D.E. Newbury, eds.). Plenum Press, New York, United States (31–75).

SHAWE, D.R. (2011) Uranium-vanadium deposits of the Slick Rock district, Colorado. *United States Geological Survey Professional Paper* **576-F**.

SHELDRICK, G.M. (2015a) *SHELXT* - Integrated space-group and crystal-structure determination. *Acta Crystallographica* **A71**, 3–8.

SHELDRICK, G.M. (2015b) Crystal Structure refinement with *SHELX*. *Acta Crystallographica* **C71**, 3–8.

Received December 20, 2017. Revised manuscript accepted March 9, 2018.